

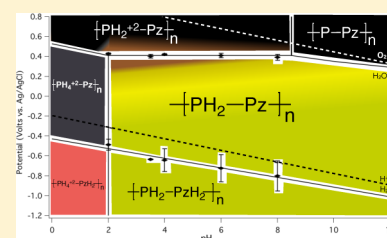
# Preparations and Electrochemical Characterizations of Conductive Porphyrin Polymers

Nicholas U. Day, Michael G. Walter,<sup>†</sup> and Carl C. Wamser\*

Department of Chemistry, Portland State University, Portland, Oregon 97207-0751, United States

## S Supporting Information

**ABSTRACT:** 5,10,15,20-Tetrakis(4-aminophenyl)porphyrin (TAPP) undergoes oxidative polymerization to form electronically conductive, nanofibrous structures in which the porphyrin units are linked by phenazine bridges. Polymerizations by chemical oxidation, electrochemical oxidation, and interfacial oxidative polymerization are described. Poly-TAPP (pTAPP) films have been characterized using scanning electron microscopy, cyclic voltammetry, electrochemical impedance spectroscopy, and UV-vis spectroscopy. The polymer morphology is consistently nanofibrous, with some differences depending on the specific synthetic method. The polymer films show distinctive electrochromism at different redox and protonation states. A Pourbaix diagram correlates the proposed redox and protonation states of the polymer with applied potential, pH, and perceived color of the film. pTAPP shows the lowest resistance to oxidative doping/dedoping at low pH and potentials between +0.4 and +0.5 V vs Ag/AgCl.



## INTRODUCTION

Porphyrins appear widely in a variety of systems, both natural and otherwise.<sup>1</sup> In particular, they are commonly used in optoelectronic applications because of their versatility in terms of light absorption and redox chemistry—properties readily tuned by substituents or metal complexation.<sup>2–7</sup> Porphyrins as components of polymers, metal–organic frameworks, or covalent organic frameworks offer a wide variety of materials properties.<sup>8</sup> The property of electronic conductivity is a valuable addition to the repertoire for porphyrins, and we have recently shown that aminophenyl-substituted porphyrins can be oxidatively electropolymerized to give conductive nanofibrous polymers.<sup>9</sup> Oxidative polymerization of 5,10,15,20-tetrakis(4-aminophenyl)porphyrin (TAPP) occurs in a manner analogous to that of aniline, except that ortho (rather than para) attacks generate linkages of redox-active phenazine/dihydrophenazine units (Figure 1). In this report, we describe a variety of oxidative methods that can be used to generate poly-TAPP (pTAPP), and the resultant polymers are characterized by their spectroscopic properties, electrochemical properties, and nanostructure.

## EXPERIMENTAL METHODS

**Materials.** 5,10,15,20-Tetrakis(4-aminophenyl)porphyrin (TAPP) was purchased from TCI America and used as received. Aniline was purchased from Sigma-Aldrich, vacuum distilled over Zn dust, and stored under inert atmosphere in a freezer. Ammonium persulfate (APS) was purchased from Mallinckrodt. Dialysis tubing was regenerated cellulose (12–14 kDa) purchased from Fisher. Fluorine-doped tin oxide (FTO) electrodes (Tek1S) were purchased from Pilkington Glass.

**Instrumentation.** UV-vis spectra were taken on a Shimadzu UV 3600 spectrophotometer. Scanning electron

microscopy (SEM) was performed on an FEI Sirion XL30 instrument, typically at 5 kV. Electrochemical and conductivity measurements were performed with a Gamry Reference 600 potentiostat. Electrochemical impedance spectroscopy (EIS) analyses were performed using Gamry Echem Analyst software. The thickness of the prepared samples was determined with a DekTak profilometer.

**Spectrophotometric Oxidative Titration of TAPP with APS.** An aqueous solution of 3.75 μM TAPP in 50 mM HCl (2.5 mL) was titrated with 2 μL aliquots of aqueous APS (5–625 mM) in 50 mM HCl. After each addition of 2 μL of APS solution, the solution was thoroughly stirred and a full spectrum (300–1200 nm) was taken.

**Preparation of pTAPP by APS Oxidation.** Nanofibers of pTAPP were prepared by adapting and optimizing Kaner's polyaniline nanofiber synthesis.<sup>10,11</sup> An aliquot of 9 mL of TAPP (0.15 mM in 100 mM HCl) and an aliquot of 1 mL of APS (3.4 mM in 100 mM HCl) were cooled to 0 °C. The two solutions were mixed at 0 °C; then without any further mixing, the solution was allowed to come to room temperature, placed in a water bath at 60 °C for 3 h, and returned to room temperature. The resultant colloidal dispersion was purified by pipetting into 12–14 kDa regenerated cellulose dialysis tubing placed in aqueous 1 mM HCl (200 mL) for 1 h. The remaining colloidal dispersion was used for further experimentation by drop-casting onto the appropriate substrate, e.g., a glass slide or a conductive FTO electrode.

**Preparation of pTAPP by Interfacial Polymerization.** Thin films of pTAPP were grown at the interface of aqueous

**Received:** March 18, 2015

**Revised:** July 1, 2015

**Published:** July 1, 2015

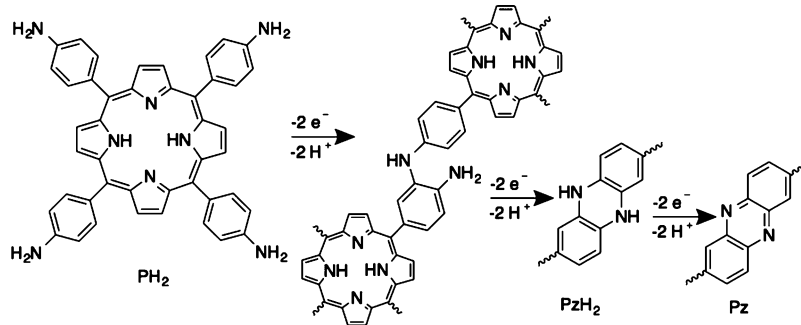


**Figure 1.** Structures showing the evolution of pTAPP via a representative dimer of TAPP (PH<sub>2</sub>), highlighting the proposed conductive linkage of dihydrophenazine (PzH<sub>2</sub>) and/or phenazine (Pz).

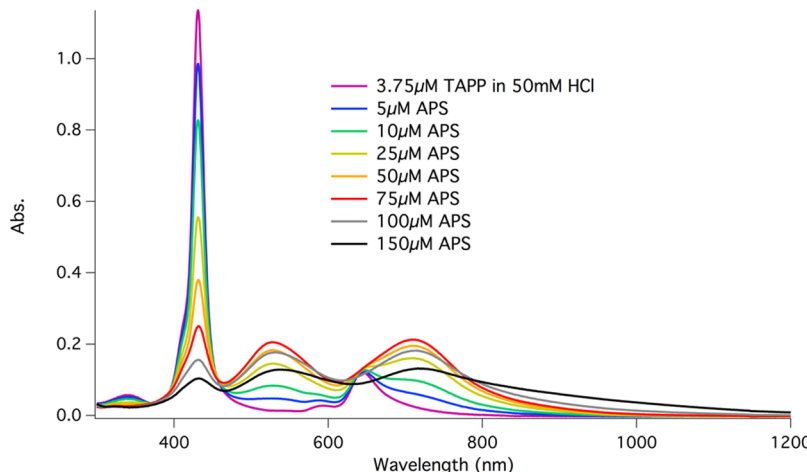


**Figure 2.** UV–vis absorption spectra of TAPP (3 mL of 3.75  $\mu$ M TAPP in 50 mM HCl) titrated with APS. The legend indicates APS concentration in the cuvette after each addition of APS.

dichloromethane (DCM) solutions using aqueous APS as oxidant and TAPP in DCM solution. In a typical experiment, an aqueous solution of 3.4 mM APS was carefully layered on top of an equal volume of 0.15 mM TAPP in DCM in a 20 mL sample vial. After 12 h, a thick black film formed at the interface leaving minimal TAPP dissolved in the DCM solution. The films were washed by replacing most of the aqueous layer with isopropyl alcohol and then harvested using an FTO conductive electrode to initially break through the side of the film, followed by scooping it out of the solution with the side of the film exposed to the aqueous/alcohol phase facing up. The films adhered well to both FTO conductive electrodes and glass microscope slides. Films could be refloated onto distilled water and rinsed with DCM and acetone. Films exhibited no visible change during storage under ambient conditions for over a year.

**Preparation of pTAPP and Polyaniline by Electrochemical Polymerization.** FTO working electrodes ( $1 \times 6$  cm) were cleaned for 10 min by sonication in Sparkleen detergent solution followed by 15 min of sonication in deionized H<sub>2</sub>O. All electrochemical preparations used a Pt flag counter electrode ( $2 \text{ cm}^2$ ) and a Ag/AgCl reference electrode. For polyaniline films the electrode was immersed in aqueous 1 M H<sub>2</sub>SO<sub>4</sub> with 0.3 M aniline and cycled between -0.2 and +0.8 V vs Ag/AgCl for 20 cycles at a rate of 20 mV/s. pTAPP films were prepared from 0.15 mM TAPP in DCM with 20 mM tetrabutylammonium perchlorate, typically using multiple cycles between 0.0 and +0.9 V and a 10 s delay at +0.9 V vs Ag/AgCl. Alternatively, pTAPP films were prepared using only a single pass from 0.0 to +0.9 V with a 10 to 150 s delay at

+0.9 V, then cycling back to +0.45 V, and finally ending at +0.6 V vs Ag/AgCl.

**Cyclic Voltammetry.** Cyclic voltammograms (CV) of pTAPP films were taken in 0.5 M KCl, electrochemical grade from Sigma-Aldrich, in Milli-Q 18 Mohm water at various pH values, adjusted with concentrated HCl or 10 M NaOH. The working electrode was a pTAPP film on an FTO electrode immersed so that no bare FTO contacted the solution. A 2 cm<sup>2</sup> Pt counter electrode along with a Ag/AgCl reference electrode were also in solution. All solutions were bubbled with nitrogen for 20 min before adjusting for each pH and again before each cycle was run. Nitrogen was blanketed over the solution during CV scans. Typical samples were run at several scan rates including 20 mV/s, 50 mV/s, 100 mV/s, and 1 V/s.

**Impedance Measurements.** Capacitance and impedance of the pTAPP films were determined by electrochemical impedance spectroscopy (EIS) with the film on FTO and in contact with aqueous 5 M NaCl with a Ag/AgCl reference electrode. All samples were run at room temperature with an excitation signal of 10 mV from 50 mHz to 1 MHz. To standardize the distance between the reference electrode and the working electrode, the reference electrode was affixed to the working electrode so that its glass frit was fixed at a uniform distance (approximately 1 mm) from the film on the working electrode for every run. EIS spectra were obtained at various bias potentials and pH values typically ranging from 0 to +0.7 V vs Ag/AgCl and pH 3 to 9.

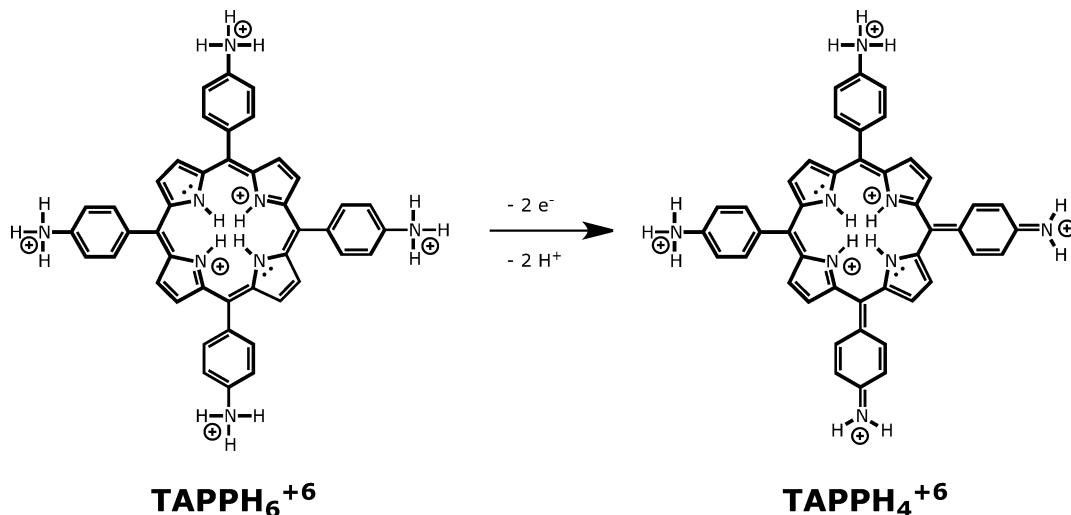


Figure 3. Proposed oxidation of fully protonated TAPP by APS in aqueous acid.

## RESULTS AND DISCUSSION

**Titration of TAPP with APS.** The oxidation of monomeric TAPP was observed by titration with aqueous APS (Figure 2). The initial spectrum of TAPP in aqueous 50 mM HCl shows a sharp Soret (B) band at 431 nm and Q bands at 593 and 645 nm, as expected for fully protonated  $\text{TAPPH}_6^{+6}$ .<sup>12</sup> APS oxidation leads to a decrease and broadening of the Soret band at 431 nm and growth of a new band at 527 nm, with an isosbestic point at 456 nm; a new peak around 710 nm grows larger and broadens during the oxidation. With excess APS, porphyrin material begins to precipitate out of solution as indicated by decreasing absorption at all of the peaks in the spectrum combined with a rising baseline indicating light scattering. The precipitation event is presumably caused by the formation of pTAPP, although at these concentrations it is not visibly detectable.

It is notable that the titrations must be performed with a great stoichiometric excess of APS in order to observe the initial oxidation. Presumably the +6 protonation state of TAPP renders it relatively resistant to oxidation. Stoichiometrically, the simplest oxidation of  $\text{TAPPH}_6^{+6}$  to  $\text{TAPPH}_4^{+6}$  would require 1 equiv of APS. Oxidative dimerization of two TAPP units to generate an oxidized phenazine linkage would require 3 equiv of APS. The most definitive spectrum (Figure 2, red) is observed when the APS concentration is about 75  $\mu\text{M}$ , which corresponds to about 20 equiv of APS relative to TAPP. This spectrum we tentatively assign to  $\text{TAPPH}_4^{+6}$ . The strong red band at 710 nm is consistent with a hyperporphyrin structure,<sup>12–15</sup> i.e., the cross-conjugation of two aminophenyl groups with the oxidized porphyrin as shown in Figure 3.

Over time, pTAPP precipitation can occur even at low concentrations of APS. Thus, the titrations were carried out quickly; presumably, the low porphyrin concentration slows the polymerization process so that it is possible to observe the oxidation process before precipitation occurs. The observation of a clean isosbestic point at 456 nm (Figure 2) suggests that this strategy is successful in the earliest stages of the titration.

**Nanostructure of pTAPP.** The predominant form of pTAPP is nanofibers in all methods of polymerization. At a macromolecular level, nanofibers can be considered the physical extension of polymer growth through a quiescent solution as monomer is depleted in the nearby environment.

Electropolymerization generates a thick interconnected web of nanofibers with diameters about 40–100 nm, as previously reported (Figure 4a).<sup>9</sup> Interfacial polymerization generates

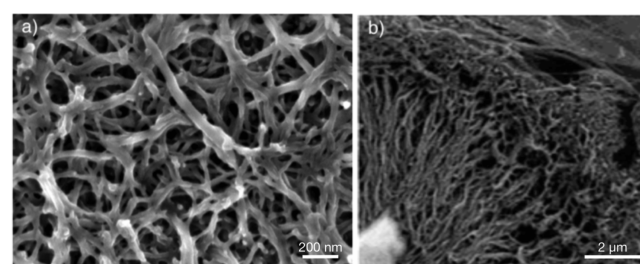


Figure 4. SEM images of nanostructured pTAPP grown by (a) electropolymerization and (b) interfacial polymerization.

spherical globules of polymer, within which nanofibers are clearly visible (Figure 4b). The globular morphology is commonly observed in interfacial polymers; it is attributed to thermal effects at the interface in which convection and density gradients cause bubble formation.<sup>16</sup>

Whereas electropolymerization or interfacial polymerization generates a thin film of polymer, generation of bulk quantities can be accomplished by chemical oxidation. Bulk oxidation of TAPP with APS was carried out in an unstirred solution at constant temperature—conditions that have been shown to facilitate nanofiber formation in polyaniline.<sup>10,11,17</sup> In order to optimize the morphology of the nanofibers, reaction conditions at room temperature were explored including concentrations, reaction time, and dialysis time.

pTAPP harvested after slow addition of oxidant, i.e., titration, showed the evolution of modified nanofibers (Figure 5). Before dialysis, the nanofibers tend to aggregate together (Figure 5a), possibly caused by the relatively high ionic strength and acidity (50 mM HCl) at that point. After overnight dialysis, the nanofibers tend to become overlaid with clumps of material (Figure 5c), possibly caused by slow continued growth of additional polymer overnight. However, if dialysis is performed quickly (1 h) and the polymer harvested, the structure is primarily well separated individual nanofibers (Figure 5b).

**Interfacial Polymerization of TAPP.** An alternative method to chemically polymerize TAPP is at an aqueous/

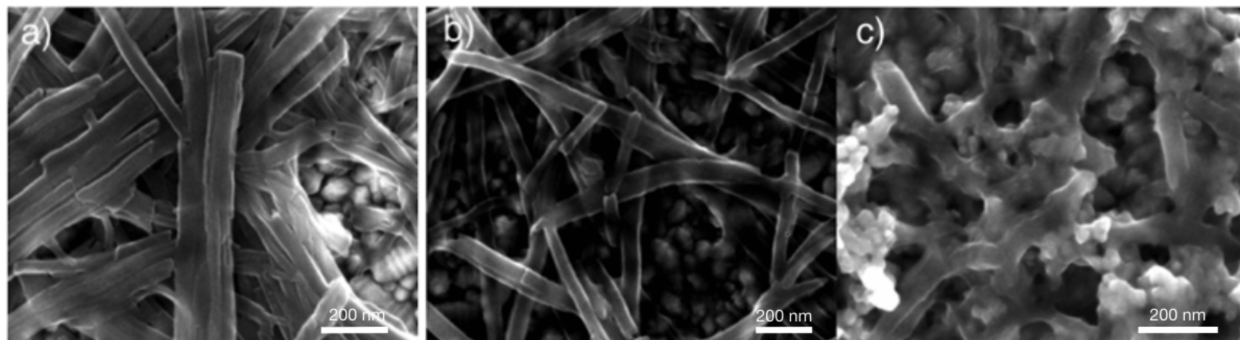


**Figure 5.** (a) SEM images of pTAPP formed by slow addition of APS, before dialysis. (b) Same preparation, after 1 h dialysis. (c) Same preparation, after overnight dialysis. The underlying granular structure is the FTO substrate.

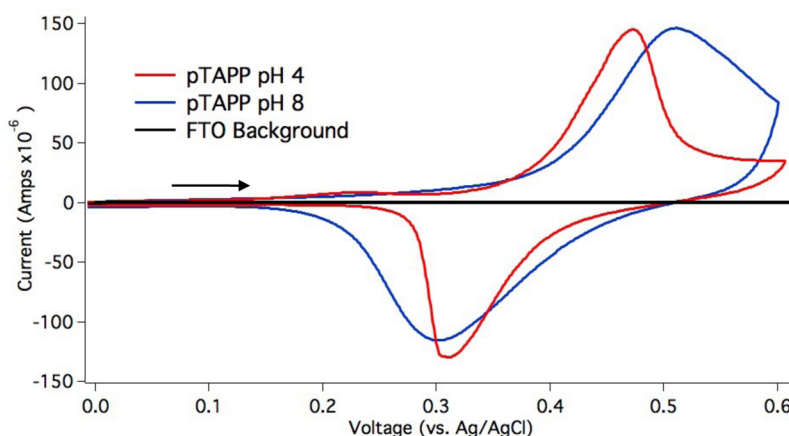


**Figure 6.** Cyclic voltammograms of a pTAPP film in aqueous 0.1 M KCl adjusted to pH 4 (red) or pH 8 (blue) at a scan rate of 20 mV/s.

organic interface. Earlier we showed that TAPP can be polymerized at an interface with several different poly(acyl chlorides), including the acid chloride derivative of 5,10,15,20-tetrakis(4-carboxyphenyl)porphyrin (TCPP).<sup>16</sup> Kaner has also shown that the interfacial polymerization technique can be used to generate polyaniline nanofibers.<sup>10,11,17</sup> Experiments were performed using 0.15 mM TAPP in DCM and an excess (8 mol equiv) of APS per TAPP dissolved in water at 3.4 mM. The results were dramatic; a thin (approximately 2  $\mu$ m), durable film was produced in 12 h at the interface accompanied by complete disappearance of TAPP in solution (see Supporting Information for Figure S1a). The black films could be harvested with an FTO electrode or a glass microscope slide, air-dried, and then handled as a free-standing film on the substrate. If the solution is not stirred, the oxidation of monomer is rapid enough to form a detectable depletion region just below the surface of the film after 2 h, and complete reaction takes about 12 h. We conclude that under unstirred conditions the rate of polymerization is controlled by TAPP monomer diffusion after the initial oxidation and film formation.

Experiments were also performed in which the lower reaction solution was gently stirred to ensure that the solution concentration remained uniform throughout. TAPP monomer concentration was monitored over time as TAPP diffuses to the interface for oxidation and polymerization. In these experiments, fresh monomer was continuously available for oxidation and polymerization, and the disappearance of monomer followed a first-order decay and was more rapid than in the unstirred case, coming to completion in about 6 h (see Supporting Information for Figure S1b).

**Cyclic Voltammetry.** pTAPP films immersed in aqueous electrolyte consistently show two major waves. The largest peak at about +0.5 V vs Ag/AgCl is attributed to the oxidation of the porphyrin units in the polymer (Figure 6). This peak occurs at a location close to where monomeric TAPP undergoes oxidation.<sup>7,9</sup> The peak shape is similar to that of an adsorbed species, which would be consistent with a conductive polymer film on the electrode. However, the polymer film is not conductive or homogeneous under all circumstances, and this leads to variable peak shapes and positions. As shown in Figure 6, the cyclic voltammogram at pH 4 presents a sharp oxidation wave with a peak at about +0.48 V. The current drops sharply after the peak because the film is substantially less conductive when in its fully oxidized form. The reverse wave at pH 4 peaks at about +0.31 V, well separated from the oxidation peak because the film is not initially conductive. In general, the positions of the oxidation waves for pTAPP do not vary significantly with pH, but their shape is quite variable depending on thickness, preparation method, and pH. The peaks are relatively broad and somewhat variable due to inhomogeneity of the polymer film, especially in its less-conductive states.

The main reduction wave occurs in the range of -0.4 to -0.7 V vs Ag/AgCl. This wave does vary with pH and is proposed to correspond to the reduction of phenazine to dihydrophenazine. The reduction of phenazine to dihydrophenazine is considered to be two one-electron processes at low pH which merge to a single two-electron process at higher pH.<sup>18</sup> We see a similar trend with the proposed phenazine reduction peaks in the polymer. The reduction at pH 4 shows two peaks, at

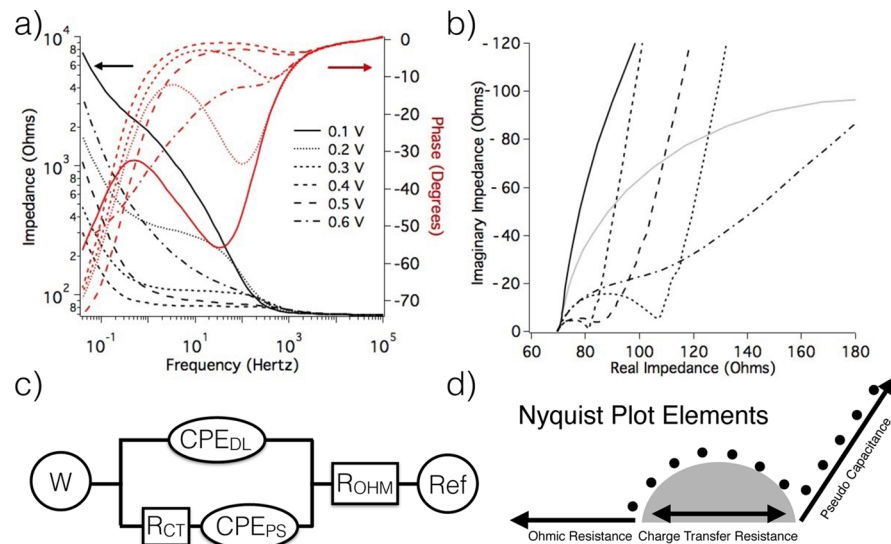


**Figure 7.** (a) Bode plots of impedance and phase shift for an electrochemically polymerized pTAPP film at pH 4. (b) Nyquist plots of the same data, where the legend for potential applies to both plots. (c) Equivalent circuit used to model the EIS data, simplified from a transmission line model (see Supporting Information for Figure S3). (d) Interpretation of the features of the Nyquist plots based on the equivalent circuit model.

approximately  $-0.5$  and  $-0.65$  V, each peak indicating a one-electron process. At pH 8, the reduction peak is a broad peak similar to that seen for the reduction of phenazine at corresponding pH values. These peaks are considerably more negative than those reported, which we believe is due to the resistive nature of the film at these potentials. The peak potential and the shape of this wave also vary significantly with the thickness and preparation method for different polymer films. Additional representative cyclic voltammograms including the negative potential range are shown in Supporting Information Figure S2.

**Electrochemical Impedance Spectroscopy.** Currently, polymers are used in a wide array of electronic applications,<sup>19,20</sup> in which electronic conductivity can be modulated using a variety of doping methods, including redox doping, acid–base chemistry, photodoping, and charge-injection doping.<sup>21,22</sup> Given the conjugated structure proposed for pTAPP, all of these doping types are conceivable. Oxidative p-doping and doping through acid–base chemistry can be clearly demonstrated for pTAPP using electrochemical impedance spectroscopy (EIS) by adjusting either bias potential or pH.

Using electrochemically grown films and following the procedures outlined by Rubinstein et al., impedance was studied over a range of potential and pH values.<sup>23</sup> In general, the lowest impedance values were observed when the film was closest to the half-wave oxidation potential (around +0.4 V vs Ag/AgCl with a scan rate of 20 mV/s). This indicates a conductivity mechanism similar to that of polyaniline, i.e., electronic conductivity through polaron hopping, in which optimum doping and minimum resistivity occur with half of the monomeric units in the oxidized form and the other half in a reduced form.<sup>21,23</sup>

**Equivalent Circuit Models.** A recent review emphasizes that polyaniline exists in numerous different nanostructured forms, quoting Alan MacDiarmid, “there are as many different types of polyaniline as there are people who make it!”<sup>17</sup> In general, conductive polymers can be formed in a wide variety of morphologies, presumably with corresponding variations in properties such as electronic behavior. A recent review of the electrochemistry of conducting polymers outlined the wide

variety of different models that have been used to describe the electrochemical behavior of conductive polymers.<sup>24</sup> A widely accepted equivalent circuit for porous films on metal electrodes is the transmission line model.<sup>25–28</sup> The generic transmission line model proposed by Fletcher for porous polymers on a metal electrode is shown in Supporting Information Figure S3a, specifically illustrating three sets of repeating units;<sup>28</sup> the simplified version used in this work is shown in Figure 7c. The fundamental elements in the complete model include resistance within the polymer due to conjugated segments ( $R_{\text{conj}}$ ) as well as resistance and capacitance due to hopping between conjugated segments ( $R_{\text{hop}}$  and  $\text{CPE}_{\text{hop}}$ ). Subsequent elements represent the polymer/solution interface with charge-transfer resistance ( $R_{\text{ct}}$ ), double-layer capacitance ( $\text{CPE}_{\text{dl}}$ ), and pseudocapacitance ( $\text{CPE}_{\text{ps}}$ ). Finally, the solution phase is represented by ohmic resistance due to ionic transport ( $R_{\text{ion}}$ ).<sup>25</sup> By using a high concentration of supporting electrolyte (5 M NaCl) and an absence of electroactive species, we intentionally minimized solution resistance and minimized redox reactions at the polymer/solution interface, i.e., leakage current.<sup>28</sup> We simplified the transmission line model by treating the repeating elements as one, giving overall bulk properties (Figure 7c and Supporting Information Figure S3b), specifically bulk charge-transfer resistance ( $R_{\text{CT}}$ ) within the film, bulk capacitance of the double layer between the polymer film and solution ( $\text{CPE}_{\text{dl}}$ ), and the pseudocapacitance of the film ( $\text{CPE}_{\text{ps}}$ ). The ohmic resistance in the film and the ionic resistance in solution are not distinguishable and are combined to a single ohmic resistance ( $R_{\text{OHM}}$ ). Polymer films on metal electrodes have often been modeled with similarly simplified equivalent circuits.<sup>23,25,28,29</sup> Constant phase elements (CPE) were used in the equivalent circuit model instead of capacitors, as is commonly done when the capacitive elements of a system are imperfect.<sup>30–32</sup>

**Bode and Nyquist Analyses of EIS Data.** Several electrochemically prepared samples of pTAPP films were tested using EIS runs with bias potential values ranging from +0.1 to +0.6 V (vs Ag/AgCl). Impedance values of the films were determined by fitting to the equivalent circuit shown in Figure 7c for both Bode and Nyquist plots. The pTAPP films analyzed in Figure 7 showed relatively constant ohmic

Table 1. Data for the pTAPP Films Analyzed and Fitted to the Equivalent Circuit Model in Figure 7

element	bias vs Ag/AgCl					
	+0.1 V	+0.2 V	+0.3 V	+0.4 V	+0.5 V	+0.6 V
$R_{\text{OHM}}$ ( $\Omega$ )	69	69	70	70	68	69
$CPE_{\text{PS}}$ ( $\text{S s}^{\alpha}$ )	0.00037	0.0021	0.0075	0.013	0.0039	0.0015
$\alpha_{\text{PS}}$	0.66	0.86	0.88	0.91	0.89	0.63
$R_{\text{CT}}$ ( $\Omega$ )	1600	252	38	13	19	68
$CPE_{\text{DL}}$ ( $\text{S s}^{\alpha}$ )	$3.9 \times 10^{-5}$	$3.7 \times 10^{-5}$	$4.0 \times 10^{-5}$	$6.7 \times 10^{-5}$	$6.5 \times 10^{-5}$	$8.1 \times 10^{-5}$
$\alpha_{\text{DL}}$	0.86	0.87	0.86	0.80	0.77	0.71
$\chi^2$	0.0018	0.0005	0.00011	0.00019	0.0026	0.0074

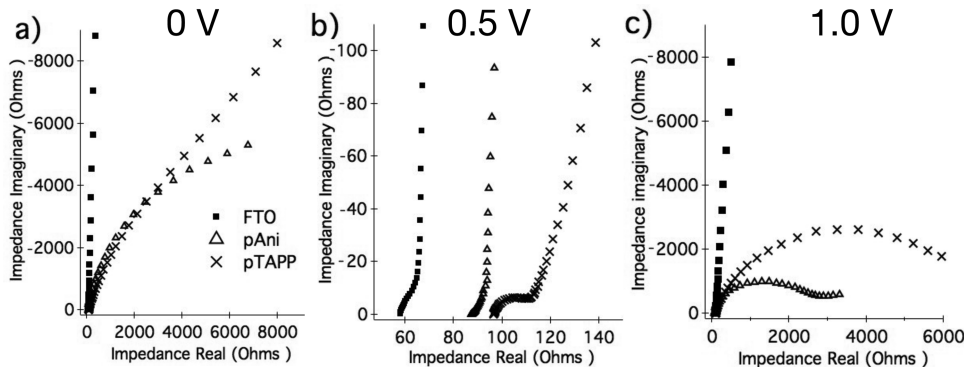


Figure 8. Nyquist plots of FTO (■), pAni (△), and pTAPP (×) showing the similarities between the conductive and insulating states at identical potentials. Graph (a) is at 0 V bias, (b) is at +0.5 V bias, and (c) is at +1.0 V bias (vs Ag/AgCl in 5 M NaCl at pH 4).

resistance ( $R_{\text{OHM}}$ ) of about 70 ohm and charge-transfer resistances ( $R_{\text{CT}}$ ) as low as 13 ohm at pH 4. Even lower impedances were observed with other films generated under different conditions, but these thicker films clearly showed the key elements in the Bode diagrams and were chosen for detailed analysis.

Figure 7a shows Bode phase plots of pTAPP films at various bias potentials. For reference, a phase of  $0^\circ$  indicates an ideal resistor, and a phase of  $-90^\circ$  indicates an ideal capacitor. The large peak seen at +0.1 V bias near 50 Hz indicates a predominantly capacitive element due to the relatively high resistance of the film at this potential. As the potential is increased to +0.4 V, this peak decreases and shifts toward 1000 Hz. Simultaneously, the impedance values decrease by almost an order of magnitude over the same frequency range. At potentials above +0.4 V, the film becomes more resistive again, and the capacitive peak begins to grow back but is less well-defined, likely due to increased leakage current through  $CPE_{\text{DL}}$  as indicated by the decreased dispersion coefficient ( $\alpha$ ).

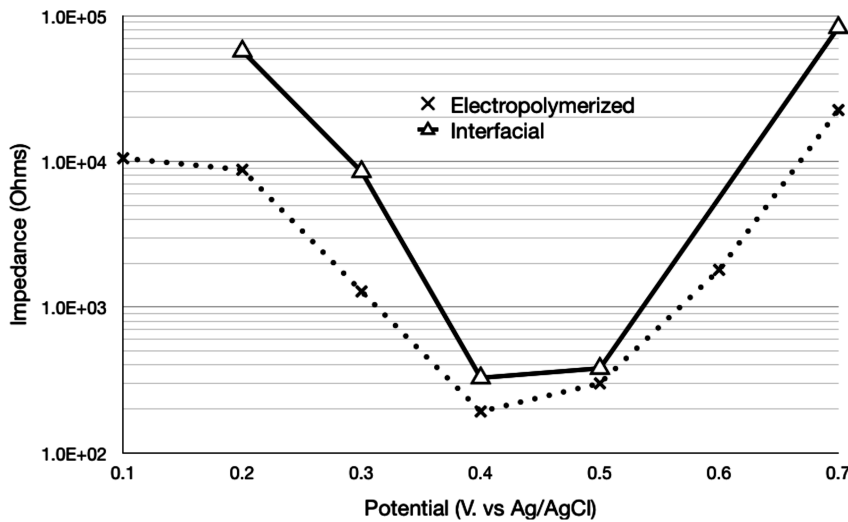
Figure 7b shows data for the identical pTAPP film and EIS runs but illustrated as Nyquist plots. Figure 7d shows the interpretation of the Nyquist plots correlated to the equivalent circuit model of Figure 7c. Unlike the Bode plots, frequencies decrease from left to right in Nyquist plots. The Nyquist plots all begin with an intercept of about 70 ohm of resistance which is indicative of the total ohmic resistance ( $R_{\text{OHM}}$ ). The RC arc which extends from 70 to 83 ohm and then to increasingly large impedance values is characteristic of the film charge-transfer resistance ( $R_{\text{CT}}$ ), indicative of the film doping/dedoping process. The smallest arc occurs at +0.4 V bias, where the film is most highly doped and  $R_{\text{CT}}$  is only 13 ohm. The charge-transfer resistance increases at both larger and smaller positive potentials.

Table 1 summarizes the results of fitting the EIS data to the equivalent circuit model, with resistance values in ohm and

CPE values in  $\text{S s}^{\alpha}$ . The data were fit using a nonlinear least-squares method.  $\chi^2$  values were determined and used to test how well the model fit the experimental data. All  $\chi^2$  values are less than  $10^{-2}$ , which represents a good fit. As the CPE elements act more like capacitors, the  $\chi^2$  fits are even better, with values less than  $10^{-3}$ .

When the dispersion coefficient,  $\alpha$ , is equal to 1, the CPE shows limiting behavior as a capacitor, and when  $\alpha$  is equal to 0.5, the CPE shows limiting behavior as a Warburg element. This is an important consideration when attempting to determine the capacitance of the film or interface.<sup>30</sup> As indicated by the relatively high values of  $\alpha$ ,  $CPE_{\text{DL}}$  can be considered to have largely a capacitive nature when potentials are between +0.1 and +0.4 V, where the values of  $CPE_{\text{DL}}$  are all relatively high. At potentials larger than +0.4 V, the capacitive nature breaks down, and there is likely an increase in leakage current. Many models of similar electroactive polymers contain a Warburg element, which does not appear to be present in our system, except possibly at higher applied potentials. Albery and Mount attribute the lack of Warburg behavior seen in polyaniline to a special case in which ionic resistance in the polymer pores is approximately equivalent to the electronic resistance to hopping between polymer segments.<sup>24,33</sup>

The pseudocapacitance ( $CPE_{\text{PS}}$ ) is largely due to redox processes within the film.<sup>23,24</sup> In order to verify the values of  $CPE_{\text{PS}}$ , the pseudocapacitance was also determined from cyclic voltammograms such as those shown in Figure 6 and Supporting Information Figure S2. Pseudocapacitance can be determined by scanning at a slow rate (20 mV/s) and dividing current by scan rate.<sup>34</sup> The pseudocapacitance calculated at the peak oxidation potential in the cyclic voltammograms had an average value of 8 mF, relatively consistent with the pseudocapacitance values determined by EIS at comparable potentials (Table 1).



**Figure 9.** Impedance values ( $R_{CT}$  from EIS Nyquist plots) for representative pTAPP films at pH 4. X markers and the dotted line represent electrochemically grown pTAPP films, and triangles and the solid line represent interfacially grown pTAPP films.

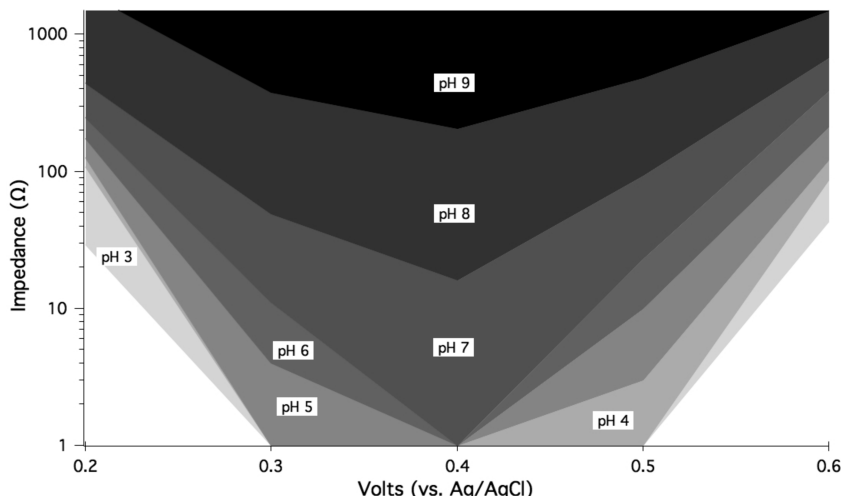


**Figure 10.** Variation in impedance values ( $R_{CT}$  from EIS Nyquist plots) for an optimized (thin) electropolymerized pTAPP film as a function of applied potential at different solution pH values.

**Comparative EIS Data for Related Systems.** Comparable EIS experiments were run on electrochemically grown polyaniline (pAni) films for comparison with pTAPP films grown similarly on FTO substrates. Figure 8 shows Nyquist plots of both types of films run at three different potentials, with bare FTO as a reference. Both polymer films exhibited similar trends at identical potentials, supporting the understanding of pTAPP as a conductive polymer similar to pAni.

Interfacially polymerized films tested under similar conditions exhibit impedance ( $R_{CT}$ ) values higher than those of electrochemically prepared films of comparable thickness. Figure 9 shows EIS impedance results ( $R_{CT}$ ) for both electrochemically and interfacially grown films of pTAPP on FTO electrodes. Both types of films showed an optimal oxidatively doped state between +0.3 and +0.5 V, but interfacially grown films show greater divergence at limiting potentials. This is likely due to increased charge-transfer resistance between the electrode and the films; interfacial films are laid upon the electrode while still wet from synthesis and rinsing steps, as compared to the electrochemical films grown directly on the electrode. In order to test this, cyclic

voltammetry of the films in a clear, monomer-free electrolyte solution was performed to visibly observe the effect on the film. Because of the electrochromic behavior of the film, discussed later, it is easy to visually detect which areas of the polymer are electrically connected. For the interfacial film, only a small amount of the black film changed color (became reduced) at the less oxidizing potentials, suggesting that only a relatively small fraction of the interfacial film is effectively connected to the electrode. Electrochemically grown pTAPP films show uniform electrochromic behavior.

**pH Effects on Polymer Electrochemical Properties.** As with polyaniline, it is expected that the conductivity of pTAPP films can be influenced by doping through acid–base chemistry.<sup>22</sup> The most conductive pTAPP samples are produced by optimizing both the potential and the pH. EIS studies were carried out with pTAPP films prepared by electropolymerization, using applied potentials between +0.2 and +0.6 V and pH values from 3 to 9 (Figure 10). Lowest values of  $R_{CT}$  are observed at a potential of about +0.4 V vs Ag/AgCl and at low pH.

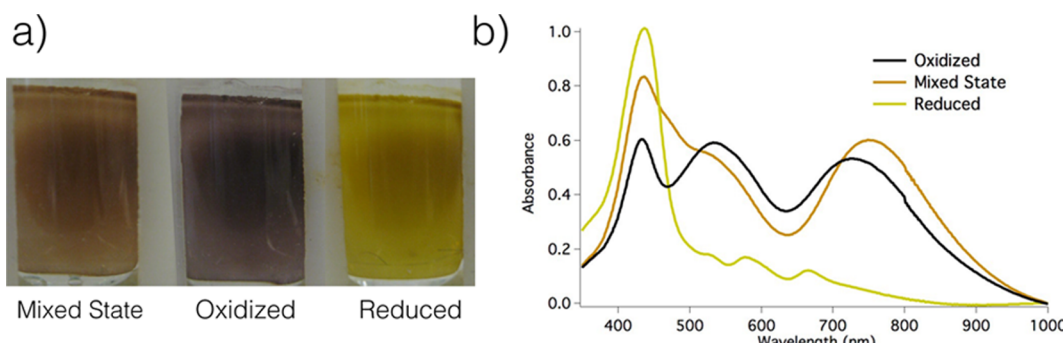


**Figure 11.** (a) Single electrochemical pTAPP film, shown in order as the reddish-brown film as synthesized, black film in 10 mM APS solution, and yellow-brown film in 10 mM ascorbic acid solution. (b) Absorbance measurements of a single pTAPP film on FTO glass. The film was synthesized electrochemically and left at a mixed state, then potentiometrically cycled to  $-0.7$  V vs Ag/AgCl to leave the film in the reduced state, and then cycled to  $+0.8$  V vs Ag/AgCl to produce the oxidized state.

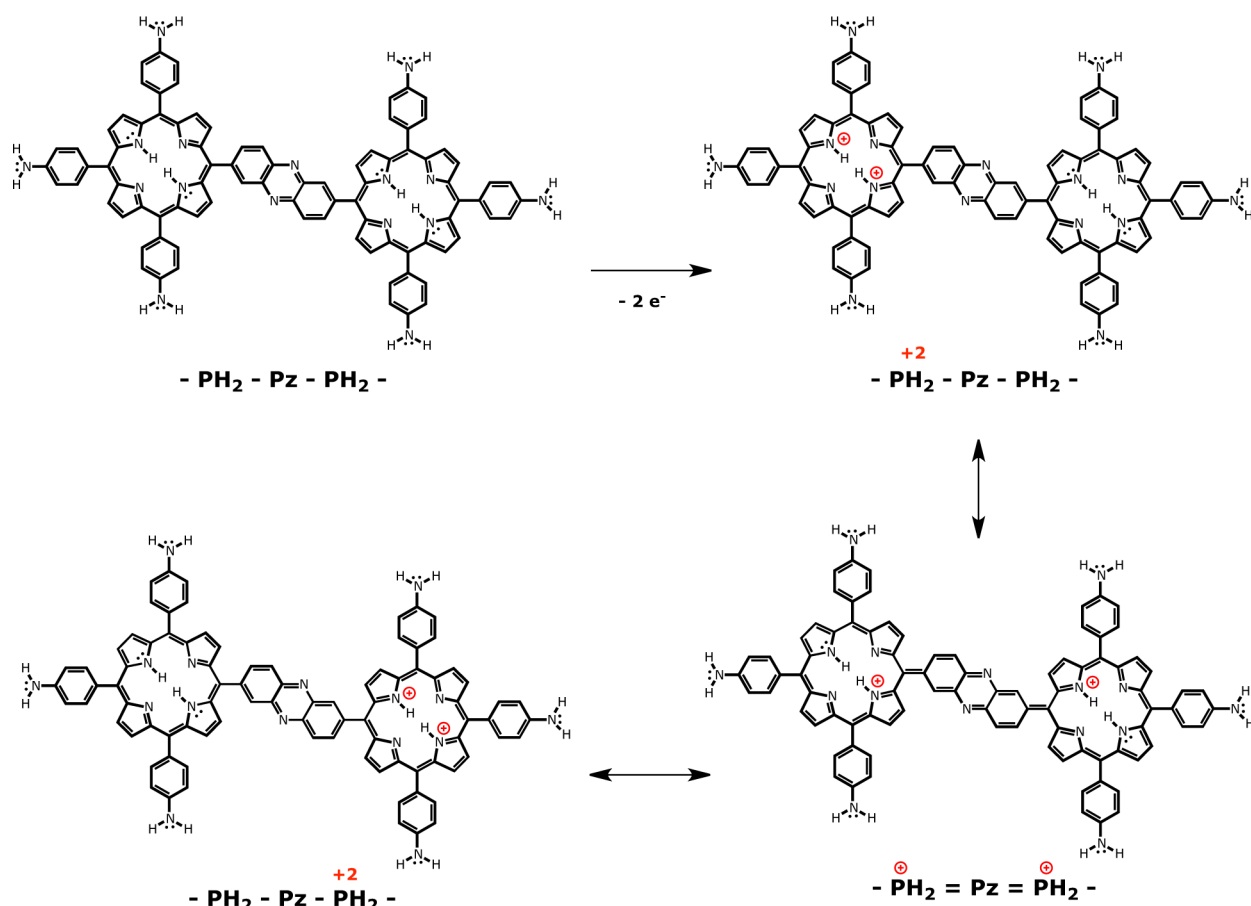


**Figure 12.** Representation of the electronic conductivity between porphyrin units via resonance forms in an oxidized TAPP dimer. All N lone pairs that are shown are part of the extended  $\pi$  system and generally are available to delocalize positive charges.

Figure 10 shows that  $R_{CT}$  values of the pTAPP film decrease at all potentials as pH decreases. Note that the minimum impedance value we could determine was about 1 ohm. The pH effect may be caused by higher concentrations of smaller, more mobile counterions ( $H^+$ ), facilitating charge transfer via hopping through the polymer. Because the  $pK_a$  of protonated phenazine is around 1.2,<sup>35</sup> it is possible that even lower  $R_{CT}$  might be observed at pH lower than 2. Although the pH effect on impedance is reversible between pH values of 3 and 9, out of this range irreversible changes occur, so that testing these films below a pH of 3 or greater than a pH of 9 is difficult.

At pH 2 and below, the film changes to a dark purple/black color. We attribute this to the protonation of the interior of the porphyrin units giving neutral porphyrin units a  $+2$  charge. The observed color is similar to the fully oxidized state of the polymer film. At pH 2, application of a potential negative enough to reduce the phenazine linkers to dihydropheophazine causes the film to turn to a red/orange color and detach from the electrode into solution.

At pH 10 and above, the film quickly undergoes a change to a green color. This is attributed to the oxidized ( $+2$ ) porphyrin units being deprotonated and returning to a neutral state.

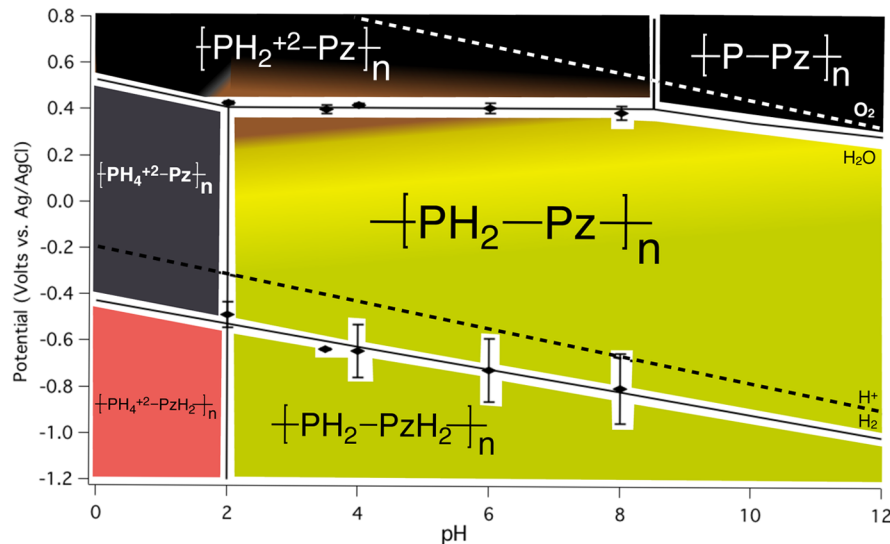


Figure 13. Pourbaix diagram showing the species present and the generalized color of pTAPP films on FTO at the given pH and potential values. Abbreviations are as shown in Figures 1 and 12.

**Electrochromic Behavior.** Electrochromic systems are currently used for a wide variety of applications and have great potential for future applications.<sup>36</sup> A distinct electrochromic behavior is observable upon oxidation and reduction of pTAPP films. This has been characterized both electrochemically and chemically, using the oxidizing agent APS and reducing agent ascorbic acid. At  $-0.7$  V vs Ag/AgCl or in ascorbic acid, the film is a golden yellow to green color, which slowly changes to reddish-brown and then a black color as more positive oxidation potentials are applied or when placed in APS. It should be noted that ascorbic acid is not powerful enough as a reductant to fully reduce the film, so that cycling to negative potentials is optimal to fully remove the strong absorbance at  $750$  nm. Figure 11 shows the film color and absorbance spectra on an FTO electrode, as synthesized (stopped at the half-wave potential of  $+0.45$  V), in the oxidized state after treatment with APS and in the reduced state after treatment with ascorbic acid. The films show reversible transitions between the three forms shown. The reduced spectra are similar to the spectra of the films at pH 10 and above while the oxidized spectra are similar to the film at pH 2 and below. Considerably different spectra are seen when strongly reducing potentials are applied to the films at low pH; the film becomes bright red and tends to come off the electrode.

**Pourbaix Diagram.** Pourbaix diagrams can be useful tools to help describe the equilibrium state of a system at a given pH and potential. In determining which species to include in the Pourbaix diagram, we applied the following data. The oxidation potential for conversion of dihydrophenazine to phenazine<sup>18,37,38</sup> occurs at potentials less positive than that of oxidation of TAPP, so we consider that the linkage between the porphyrin units is in the oxidized (phenazine) form. Phenazine is a very weak base with reported  $pK_a$  values for the diprotonated and monoprotonated species as  $-4$  and  $1.2$ .<sup>35,39</sup> Thus, the linker is represented as unprotonated phenazine at all pH and potential values studied. Interestingly, the polymer film becomes unstable at very low pH and highly negative potentials, as discussed earlier, suggesting that reduced phenazine may facilitate depolymerization or other solubilization of the polymer film. The general scheme that describes the

conductivity of the polymer film is illustrated, using a representative dimer of TAPP (Figure 12).

Considering the electrochromic behavior of pTAPP, we thought it would be convenient to generate a Pourbaix diagram that also correlates the perceived color of the film with the pH and potential range in which that system exists (Figure 13).

In a Pourbaix diagram, a vertical line can be considered to delineate a process dependent only on pH, typically correlating with the  $pK_a$  of a species. The apparent  $pK_a$  of TAPP has been determined to be between  $2$  and  $3$  in aqueous solutions as indicated by its solubility. Since the reported  $pK_a$  of phenazine is  $1.2$ ,<sup>35</sup> the acid–base color change observed near pH 2 is postulated to be that of free-base porphyrin, i.e.,  $-[\text{PH}_2-\text{Pz}]_n$  to  $-[\text{PH}_4^{2+}-\text{Pz}]_n$ . Protonated TAPP generates a strong hyperporphyrin spectrum<sup>12–14</sup> similar to that observed for oxidized TAPP or oxidized pTAPP.

Horizontal lines in a Pourbaix diagram correlate to a change dependent only on potential. The oxidation of pTAPP at about  $+0.5$  V behaves in this way at all pH values tested and would appear to be completely independent of the protonation state. On the other hand, the reduction of the polymer films shows a multiple electron/proton transition that does vary with pH. The reduction of pTAPP shows a slope of  $49$  mV per pH unit where a single electron/proton coupled process would give a slope of  $59$  mV per pH unit. We observe that the reduction of phenazine to dihydrophenazine is considerably variable, which we attribute to the neutral polymer being in an inhomogeneous and relatively resistive state.

Transitions outside of a pH range of  $2$ – $8$  are not readily observed but are added to the diagram for completeness. The oxidation of the protonated porphyrin would be increasingly difficult, and we expect the transition from  $-[\text{PH}_4^{2+}-\text{Pz}]_n$  to  $-[\text{PH}_2^{2+}-\text{Pz}]_n$  to be a two-electron and two-proton process. Likewise, the oxidation of porphyrin from  $-[\text{PH}_2^{2+}-\text{Pz}]_n$  to  $-[\text{P}^{2+}-\text{Pz}]_n$  would also be a two-electron and two-proton process. The  $pK_a$  of  $-[\text{PH}_2^{2+}-\text{Pz}]_n$  to  $-[\text{P}-\text{Pz}]_n$  is placed at approximately  $8$  in order to correlate with the transition observed at higher pH. Note that the lowest  $R_{CT}$  values (highest conductivity) occurs with the presence of a mixed state, depicted by the brownish color in the Pourbaix diagram. Coexistence of both  $-[\text{PH}_2-\text{Pz}]_n$  and  $-[\text{PH}_2^{2+}-\text{Pz}]_n$  (i.e.,

at +0.4 V, pH 2–8) is analogous to the half-oxidized emeraldine salt form of polyaniline that shows maximum conductivity.

## CONCLUSIONS

Tetra(4-aminophenyl)porphyrin can be oxidatively polymerized with a variety of methods, including electropolymerization, chemical oxidation, and interfacial polymerization. Poly-TAPP displays a nanofibrous morphology and interesting properties of electroactivity and electrochromism. Charge-transfer resistance (oxidative doping and dedoping) can be very low under optimum conditions at pH 4 and +0.4 V vs Ag/AgCl, where we propose a mixed state of neutral and oxidized porphyrin units exist in the polymer, electronically connected by phenazine bridges. Data collected from cyclic voltammetry and electrochemical impedance spectroscopy allowed us to create a novel polymer Pourbaix diagram correlating the proposed states of the system with observed color, pH, and potential.

## ASSOCIATED CONTENT

### Supporting Information

Interfacial polymerization of pTAPP films, cyclic voltammograms of pTAPP films, and transmission line model EIS simplification. The Supporting Information is available free of charge on the ACS Publications website at DOI: 10.1021/acs.jpcc.5b02628.

## AUTHOR INFORMATION

### Corresponding Author

\*E-mail wamserc@pdx.edu (C.C.W.).

### Present Address

<sup>†</sup>Department of Chemistry, University of North Carolina at Charlotte, Charlotte, North Carolina 28223, United States.

### Notes

The authors declare no competing financial interest.

## ACKNOWLEDGMENTS

Support from the Oregon Nanoscience and Microtechnologies Institute (ONAMI) and the National Science Foundation (Grant CHE-0911186) is gratefully acknowledged. Some experimental work was carried out by Kalana W. Jayawardena. We acknowledge helpful discussions regarding electrochemistry with Professor Erik Johansson as well as helpful insights from a reviewer regarding EIS interpretations.

## REFERENCES

- (1) Kadish, K. M.; Smith, K. M.; Guillard, R. *Handbook of Porphyrin Science: With Applications to Chemistry, Physics, Materials Science, Engineering, Biology, and Medicine*; World Scientific: Singapore, 2010; Vol. 1–35.
- (2) Walter, M. G.; Rudine, A. B.; Wamser, C. C. Porphyrins and Phthalocyanines in Solar Photovoltaic Cells. *J. Porphyrins Phthalocyanines* **2010**, *14*, 759–792.
- (3) Campbell, W. M.; et al. Highly Efficient Porphyrin Sensitizers for Dye-Sensitized Solar Cells. *J. Phys. Chem. C* **2007**, *111*, 11760–11762.
- (4) Alstrum-Acevedo, J. H.; Brenneman, M. K.; Meyer, T. J. Chemical Approaches to Artificial Photosynthesis. *Inorg. Chem.* **2005**, *44*, 6802–6827.
- (5) Campbell, W. M.; Burrell, A. K.; Officer, D. L.; Jolley, K. W. Porphyrins as Light Harvesters in the Dye-Sensitised TiO<sub>2</sub> Solar Cell. *Coord. Chem. Rev.* **2004**, *248*, 1363–1379.
- (6) Gust, D.; Moore, T. A.; Moore, A. L. Mimicking Photosynthetic Solar Energy Transduction. *Acc. Chem. Res.* **2001**, *34*, 40–48.
- (7) Ransdell, R. A.; Wamser, C. C. Solvent and Substituent Effects on the Redox Properties of Free-Base Tetraphenylporphyrins in DMSO and Aqueous DMSO. *J. Phys. Chem.* **1992**, *96*, 10572–10575.
- (8) Day, N. U.; Wamser, C. C.; Walter, M. G. Porphyrin Polymers and Organic Frameworks. *Polym. Int.* **2015**, *64*, 833–857.
- (9) Walter, M. G.; Wamser, C. C. Synthesis and Characterization of Electropolymerized Nanostructured Aminophenylporphyrin Films. *J. Phys. Chem. C* **2010**, *114*, 7563–7574.
- (10) Huang, J.; Kaner, R. B. A General Chemical Route to Polyaniline Nanofibers. *J. Am. Chem. Soc.* **2004**, *126*, 851–855.
- (11) Huang, J.; Virji, S.; Weiller, B. H.; Kaner, R. B. Polyaniline Nanofibers: Facile Synthesis and Chemical Sensors. *J. Am. Chem. Soc.* **2003**, *125*, 314–315.
- (12) Weinkauf, J. R.; Cooper, S. W.; Schweiger, A.; Wamser, C. C. Substituent and Solvent Effects on the Hyperporphyrin Spectra of Diprotonated Tetraphenylporphyrins. *J. Phys. Chem. A* **2003**, *107*, 3486–3496.
- (13) Wang, C.; Wamser, C. C. Hyperporphyrin Effects in the Spectroscopy of Protonated Porphyrins with 4-Aminophenyl and 4-Pyridyl Meso Substituents. *J. Phys. Chem. A* **2014**, *118*, 3605–3615.
- (14) Rudine, A. B.; DelFatti, B. D.; Wamser, C. C. Spectroscopy of Protonated Tetraphenylporphyrins with Amino/carbomethoxy Substituents: Hyperporphyrin Effects and Evidence for a Monoprotonated Porphyrin. *J. Org. Chem.* **2013**, *78*, 6040–6049.
- (15) Ojadi, E. C. A.; Linschitz, H.; Gouterman, M.; Walter, R. I.; Lindsey, J. S.; Wagner, R. W.; Droupadi, P. R.; Wang, W. Sequential Protonation of Meso-[p-(dimethylamino)phenyl]porphyrins: Charge-Transfer Excited States Producing Hyperporphyrins. *J. Phys. Chem.* **1993**, *97*, 13192–13197.
- (16) Li, W.; Wamser, C. C. Synthesis and Characterization of Interfacially Polymerized Films of Tetraphenylporphyrin Derivatives. *Langmuir* **1995**, *11*, 4061–4071.
- (17) Tran, H. D.; D'Arcy, J. M.; Wang, Y.; Beltramo, P. J.; Strong, V. A.; Kaner, R. B. The Oxidation of Aniline to Produce "Polyaniline": A Process Yielding Many Different Nanoscale Structures. *J. Mater. Chem.* **2011**, *21*, 3534–3550.
- (18) Bailey, D. N.; Hercules, D. M.; Roe, D. K. Electrochemistry and Photopotentials of Phenazine in Methanol Solutions. *J. Electrochem. Soc.* **1969**, *116*, 190–195.
- (19) Cirić-Marjanović, G. Recent Advances in Polyaniline Research: Polymerization Mechanisms, Structural Aspects, Properties and Applications. *Synth. Met.* **2013**, *177*, 1–47.
- (20) Das, T. K.; Prusty, S. Review on Conducting Polymers and Their Applications. *Polym.-Plast. Technol. Eng.* **2012**, *51*, 1487–1500.
- (21) MacDiarmid, A. G. "Synthetic Metals": A Novel Role for Organic Polymers (Nobel Lecture). *Angew. Chem., Int. Ed.* **2001**, *40*, 2581–2590.
- (22) Heeger, A. J. Nobel Lecture: Semiconducting and Metallic Polymers: The Fourth Generation of Polymeric Materials. *Rev. Mod. Phys.* **2001**, *73*, 681–700.
- (23) Rubinstein, I.; Sabatani, E.; Rishpon, J. Electrochemical Impedance Analysis of Polyaniline Films on Electrodes. *J. Electrochem. Soc.* **1987**, *134*, 3078–3083.
- (24) Robinson, J. F.; Kayinamura, Y. P. Charge Transport in Conducting Polymers. *Chem. Soc. Rev.* **2009**, *38*, 3339–3347.
- (25) Mondal, S. K.; Prasad, K. R.; Munichandraiah, N. Analysis of Electrochemical Impedance of Polyaniline Films Prepared by Galvanostatic, Potentiostatic, and Potentiodynamic Methods. *Synth. Met.* **2005**, *148*, 275–286.
- (26) Garcia-Belmonte, G.; Bisquert, J.; Pereira, E. C.; Fabregat-Santiago, F. Anomalous Transport on Polymeric Porous Film Electrodes in the Dopant-Induced Insulator-to-Conductor Transition Analyzed by Electrochemical Impedance. *Appl. Phys. Lett.* **2001**, *78*, 1885–1887.
- (27) Bisquert, J.; Garcia-Belmonte, G.; Bueno, P.; Longo, E.; Bulhões, L. O. S. Impedance of Constant Phase Element (CPE)-Blocked Diffusion in Film Electrodes. *J. Electroanal. Chem.* **1998**, *452*, 229–234.

- (28) Fletcher, S. Contribution to the Theory of Conducting-Polymer Electrodes in Electrolyte Solutions. *J. Chem. Soc., Faraday Trans.* **1993**, *89*, 311–320.
- (29) Sarac, A. S.; Murat, A.; Bilge, K. Electrochemical Impedance Spectroscopic Study of Polyaniline on Platinum, Glassy Carbon, and Carbon Microelectrodes. *Int. J. Electrochem. Sci.* **2008**, *3*, 777–786.
- (30) Jorcin, J.-B.; Orazem, M. E.; Pébère, N.; Tribollet, B. CPE Analysis by Local Electrochemical Impedance Spectroscopy. *Electrochim. Acta* **2006**, *S1*, 1473–1479.
- (31) Córdoba-Torres, P.; Mesquita, T. J.; Nogueira, R. P. Relationship between the Origin of Constant-Phase Element Behavior in Electrochemical Impedance Spectroscopy and Electrode Surface Structure. *J. Phys. Chem. C* **2015**, *119*, 4136–4147.
- (32) Zoltowski, P. On the Electrical Capacitance of Interfaces Exhibiting Constant Phase Element Behaviour. *J. Electroanal. Chem.* **1998**, *443*, 149–154.
- (33) Albery, W. J.; Mount, A. R. Dual Transmission Line with Charge-transfer Resistance for Conducting Polymers. *J. Chem. Soc., Faraday Trans.* **1994**, *90*, 1115–1119.
- (34) Li, H.; Wang, J.; Chu, Q.; Wang, Z.; Zhang, F.; Wang, S. Theoretical and Experimental Specific Capacitance of Polyaniline in Sulfuric Acid. *J. Power Sources* **2009**, *190*, 578–586.
- (35) Albert, A.; Goldacre, R.; Phillips, J. The Strength of Heterocyclic Bases. *J. Chem. Soc.* **1948**, 2240–2249.
- (36) Monk, P.; Mortimer, R.; Rosseinsky, D. *Electrochromism and Electrochromic Devices*; Cambridge University Press: Cambridge, UK, 2007.
- (37) Dong, Q.; Su, J.-H.; Gong, S.; Li, Q.-S.; Zhao, Y.; Wu, B.; Yang, X.-J. Nickel Complexes with Two Types of Noninnocent Ligands:  $\alpha$ -Diimine and Phenazine. *Organometallics* **2013**, *32*, 2866–2869.
- (38) Kaye, R. C.; Stonehill, H. I. The Polarographic Reduction of Pyridine, Quinoline, and Phenazine. *J. Chem. Soc.* **1952**, 3240–3243.
- (39) Laviron, E.; Roullier, L. Electrochemical Reactions with Protonations at Equilibrium: Part IX. Comparison between the Surface and Heterogeneous Electrochemical Rate Constants in the System Phenazine/Dihydrophenazine. *J. Electroanal. Chem. Interfacial Electrochem.* **1983**, *157*, 7–18.